

Spin-Phonon Relaxation in Molecular Qubits from First Principles Spin Dynamics

¹Alessandro Lunghi* and ¹Stefano Sanvito

¹*School of Physics, AMBER and CRANN, Trinity College, Dublin 2, Ireland*

The coupling between electronic spins and lattice vibrations is fundamental for driving relaxation in magnetic materials. The debate over the nature of spin-phonon coupling dates back to the 40's, but the role of spin-spin, spin-orbit and hyperfine interactions, has never been fully established. Here we present a comprehensive study of the spin dynamics of a crystal of Vanadyl-based molecular qubits by means of first-order perturbation theory and first-principles calculations. We quantitatively determine the role of the Zeeman, hyperfine and electronic spin dipolar interactions in the direct mechanism of spin relaxation. We show that, in a high magnetic field regime, the modulation of the Zeeman Hamiltonian by the intra-molecular components of the acoustic phonons dominates the relaxation mechanism. In low fields, hyperfine coupling takes over, with the role of spin-spin dipolar interaction remaining the less important for the spin relaxation.

Spin 1/2 systems represent the fundamental prototype of magnetic materials and the understanding of their properties is pivotal for the rationalization of any more complex magnetic compound. Their study has deep roots in the early days of quantum mechanics and, despite their basic nature, they still represent a very rich quantum playground with non-trivial and elusive dynamical properties. The spin life-time in insulating materials is essentially limited by the interaction between spins and lattice vibrations, namely the spin-phonon coupling. At finite temperature, spins can absorb/emit one or multiple phonons from/into the lattice and relax to an equilibrium state. The detailed understanding of this process at the first-principles level represents a long-standing question in physics and chemistry and goes well beyond the fundamental-theory aspect.

Spin-lattice relaxation is key in several fields. For instance, the efficiency of magnetic-resonance-imaging contrast agents [1] and the spin life-time of single molecule magnets [2] is determined by the magnetization decay rate of paramagnetic elements. Turning to the main focus of this work, in both molecular and solid-state qubits, spin-lattice relaxation sets the upper limit for the coherence time [3–6] and the engineering of this interaction is a primary challenge in the spin-based quantum computing field. The synthetic versatility of molecular compounds offers an intriguing route to the tailoring of spin-phonon coupling but needs to be supported by a rational understanding of the physical principles governing spin relaxation.

The debate over the role of phonons in the relaxation of electronic spins can be traced back to the 40's, when it was discussed for the first time in the context of transition-metal chemistry. Relaxation pathways occurring through the modulation of spin dipolar interactions or the modulation of the *d*-electrons' crystal field were firstly pointed out by Waller [7] and Van Vleck [8, 9],

respectively. More recently, the role of hyperfine interaction has also been discussed [10]. Van Vleck's mechanism remains to date the most commonly accepted explanation for the microscopic origin of spin-lattice relaxation of electronic spins. Several questions, however, remain unanswered. In particular, early models, being phenomenological, could not entirely address the nature of the coupling between phonons and spins and simply ascribe acoustic vibrations as responsible for this interaction. Molecular compounds are inherently complex and a rational description of spin relaxation in terms of molecular motions is still to be developed.

First-principles calculations represent the perfect ground to provide unbiased answers to such fundamental questions. The possibility to predict the spin-relaxation times in magnetic materials without introducing any phenomenological parameter is also of fundamental importance from a materials-design perspective. Quantum chemistry and related disciplines have been already proved to be invaluable tools for providing insights into the physics of new chemical systems [11] and they have been used as a screening method to predict new materials with tailored properties [12]. These computational strategies represent a rich opportunity for the field of quantum informatics. The development of a first-principle framework able to predict the spin-relaxation time is the first step in that direction. In this work we offer a theoretical and computational explanation of the nature of the atomistic processes that lead to the relaxation of a molecular electronic $S = 1/2$ system.

Our approach builds on previous contributions from ourselves [13, 14] and others [15–18] and significantly extends the state of the art in the field. For the first time we include in the formulation the contribution of phonons from the entire Brillouin zone and the hyperfine and dipolar spin-spin interactions, both at a static and dynamical level. The description of all the fundamental spin-relaxation channels occurring at the first-order of perturbation theory is therefore here complete. Our method is purely first-principle and provides a rationalization of spin-lattice relaxation with-

* lunghia@tcd.ie

out any previous knowledge of the system's properties other than its crystal structure. The $S = 1/2$ system investigated is the crystal of the Vanadyl complex $\text{VO}(\text{acac})_2$, being $\text{acac}=\text{acetylacetonate}$ [19]. Vanadyl-based molecular qubits represent archetypal systems for room-temperature quantum-computing applications [20].

We demonstrate that Van Vleck's mechanism is the dominant first-order relaxation channel for $S = 1/2$ molecular spins in a high magnetic field, while hyperfine contributions become dominant in a low-field regime. Most importantly, our calculations show that acoustic phonons are not rigid molecular translations, shedding light on the origin of spin-phonon coupling in solid-state spin $1/2$ compounds, and thus solving a eighty-year-old controversy.

I. RESULTS

A. First-Principles Spin Dynamics

The quantum dynamics of even a single spin is, in principle, entangled with the dynamics of all the other spin and lattice degrees of freedom that it is interacting with. More explicitly, it is driven by the total Hamiltonian $H = H_s + H_{\text{ph}} + H_{\text{sph}}$, where the three terms are, respectively, the spins and phonons Hamiltonian, and the spin-phonon coupling. It is convenient to think at the problem as composed of two parts: the simulation of the sole spin degrees of freedom as an isolated system and the interaction of this ensemble with a thermal bath, namely with the phonons.

The spin Hamiltonian of Eq. (1) describes the fundamental interactions taking place within an ensemble of N_s spins,

$$\hat{H}_s = \sum_i^{N_s} \beta_i \vec{\mathbf{B}} \cdot \mathbf{g}(i) \cdot \vec{\mathbf{S}}(i) + \frac{1}{2} \sum_{ij}^{N_s} \vec{\mathbf{S}}(i) \cdot \mathbf{D}(ij) \cdot \vec{\mathbf{S}}(j), \quad (1)$$

where the i -th spin, $\mathbf{S}(i)$, interacts with an external magnetic field $\vec{\mathbf{B}}$ through the gyromagnetic tensor, $\beta \mathbf{g}(i)$. Eq. (1) can account for both electronic and nuclear spins on the same footing. Thus the spin-spin interaction tensor, \mathbf{D} , may coincide with the point-dipole interaction, \mathbf{D}^{dip} , or the hyperfine tensor, \mathbf{A} , depending on whether the interaction is among electronic and/or nuclear spins. The state of the spin system can be described in term of the spin density matrix, $\hat{\rho}$, whose dynamics is regulated by the Liouville equation,

$$\frac{d\hat{\rho}}{dt} = -\frac{i}{\hbar} [\hat{H}_s, \hat{\rho}]. \quad (2)$$

Once the eigenstates and eigenvalues, $\{E_a\}$, of the spin Hamiltonian are known, it is possible to integrate exactly Eq. (2) and obtain an expression for the time evolution of ρ_{ab}^{I} in the so-called configuration interaction,

$$\rho_{ab}^{\text{I}}(t) = e^{-i\omega_{ab}(t-t_0)} \rho_{ab}(t_0), \quad (3)$$

where $\omega_{ab} = (E_a - E_b)/\hbar$. Despite its simple form, Eq. (3) hides a high level of complexity, which originates from the high dimension of the Hilbert space it acts on. Several numerical schemes exist to reduce the computational costs associated to this problem [21, 22] and these will be the subject of future investigations. Here we have decided to retain the full Hilbert space description and restrict the study to a small number of interacting spins.

The basic theory for phonon-driven spin relaxation has been derived before [13, 14]. Here we extend it by including acoustic phonons and the phonon reciprocal space dispersion. For a periodic crystal, defined by a set of reciprocal lattice vectors, \mathbf{q} , and by N atoms in the unit-cell, the lattice's dynamics can be described in terms of periodic displacement waves (phonons), $Q_{\alpha\mathbf{q}}$, with frequency $\omega_{\alpha\mathbf{q}}$ and obeying to an harmonic Hamiltonian

$$\hat{H}_{\text{ph}} = \sum_{\alpha\mathbf{q}} \hbar\omega_{\alpha\mathbf{q}} (\hat{n}_{\alpha\mathbf{q}} + 1). \quad (4)$$

Here $\hat{n}_{\alpha\mathbf{q}}$ is the phonon's number operator. The spin-phonon coupling Hamiltonian, responsible for the energy exchange between the spins and the lattice, writes

$$H_{\text{sph}} = \sum_{\alpha\mathbf{q}} \left(\frac{\partial H_s}{\partial Q_{\alpha\mathbf{q}}} \right) Q_{\alpha\mathbf{q}}. \quad (5)$$

Usually, phonons dynamics develops at a time scale much shorter than that of the spin relaxation. Therefore, if no phonon bottleneck is at play, the Born-Markov approximation will be valid and the phonons dynamics can be considered to be always at the thermal equilibrium. Under these circumstances the full set of Redfield equations can be used to study the spin dynamics under the effect of a phonon bath [23]. In this framework, the spin density matrix $\rho_{ab}^{\text{I}}(t)$ evolves according to the equation,

$$\frac{d\rho_{ab}^{\text{I}}}{dt} = \sum_{cd} \sum_{\alpha\mathbf{q}} R_{ab,cd}^{\alpha\mathbf{q}} \rho_{cd}^{\text{I}}(t). \quad (6)$$

The transition rates between the elements of the density matrix are of the form

$$R_{ab,cd}^{\alpha\mathbf{q}} \propto \frac{\pi}{2\hbar^2} V_{ac}^{\alpha\mathbf{q}} V_{db}^{\alpha\mathbf{q}} \left(G(\omega_{db}, \omega_{\alpha\mathbf{q}}) + G(\omega_{cd}, \omega_{\alpha\mathbf{q}}) \right), \quad (7)$$

where $V_{ab}^{\alpha\mathbf{q}} = \langle a | \frac{\partial H_s}{\partial Q_{\alpha\mathbf{q}}} | b \rangle$ is the matrix element of the spin-phonon Hamiltonian in the spin Hamiltonian eigenfunctions basis and $G(\omega_{ij}, \omega_{\alpha\mathbf{q}})$ is the single phonon correlation function at finite temperature. For harmonic lattices, $G(\omega_{ij}, \omega_{\alpha\mathbf{q}})$ is defined as

$$G(\omega_{ij}, \omega_{\alpha\mathbf{q}}) = \bar{n}_{\alpha\mathbf{q}} \delta(\omega_{\alpha\mathbf{q}} - \omega_{ij}) + (\bar{n}_{\alpha\mathbf{q}} + 1) \delta(\omega_{\alpha\mathbf{q}} + \omega_{ij}), \quad (8)$$

where $\bar{n}_{\alpha\mathbf{q}}$ is the Bose-Einstein population at a temperature T . Once Eq. (6) is solved, the magnetization dynamics for the i -th spin can be computed by the canonical expression $\vec{\mathbf{M}}(i) = \text{Tr}\{\hat{\rho}(t)\vec{\mathbf{S}}(i)\}$.

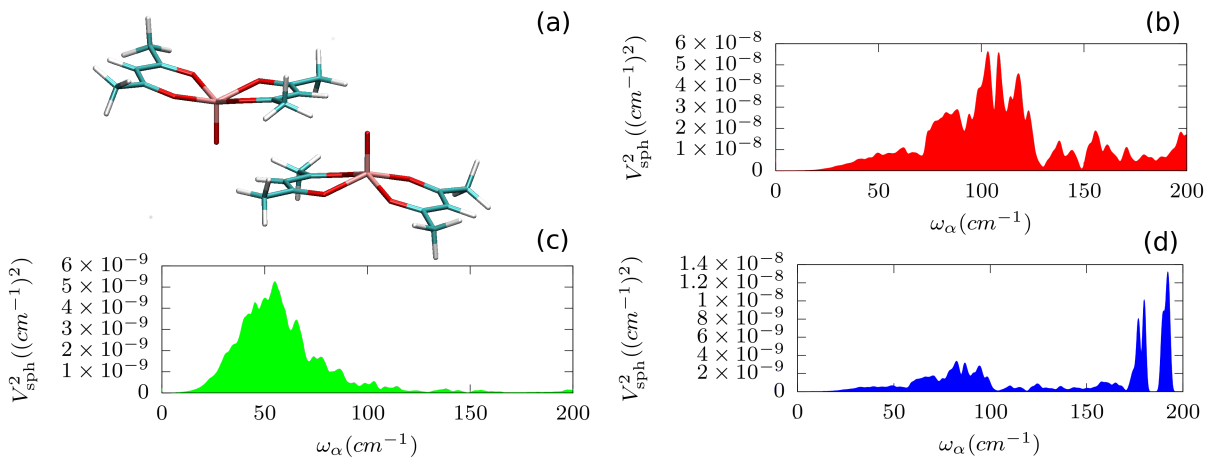


FIG. 1. **VO(acac)₂ structure and spin phonon coupling distributions.** Panel (a) shows the geometrical structure of the two VO(acac)₂ molecular units inside the crystal’s unit-cell. Vanadium atoms are represented in pink, oxygen in red, carbon in green and hydrogen in white. Panel (b) shows the spin-phonon coupling distribution relative to the Zeeman energy as function of the phonons’ frequency. Panel (c) shows the spin-phonon coupling distribution relative to the dipolar spin-spin energy as function of the phonons’ frequency. Panel (d) shows the spin-phonon coupling distribution relative to the hyperfine energy as function of the phonons’ frequency.

B. Spin Phonon Coupling in Molecular Qubits

In order to make the physics of Eq. (7) more transparent, a study of the spin-phonon coupling terms, V_{ab} , for the molecular qubit VO(acac)₂ is hereafter provided. This V⁴⁺ complex crystallises with a triclinic primitive cell containing two inversion-symmetry-related molecular units [19], as reported in Fig. 1. Each molecule bears a single electronic $S = 1/2$ spin in addition to the $I = 7/2$ nuclear spin of ⁵¹V. Let us consider one electronic spin \vec{S}_i interacting with the rest of the crystal electronic spins \vec{S}_j and the local vanadium nuclear spin \vec{I}_i . Given the definition in Eq. (5), the spin-phonon coupling Hamiltonian will contain three distinguished contributions: a first intra-molecular spin-phonon coupling due to the modulation of the Landé tensor, \mathbf{g} ; a second intra-molecular coupling coming from the modulation of the hyperfine interaction, \mathbf{A} ; and an inter-electronic spins interaction originating from the modulation of the dipolar terms, \mathbf{D}^{dip} , namely

$$\begin{aligned} \frac{\partial H_s(i)}{\partial Q_{\alpha\mathbf{q}}} = & \beta_i \vec{\mathbf{B}} \cdot \frac{\partial \mathbf{g}(i)}{\partial Q_{\alpha\mathbf{q}}} \cdot \vec{\mathbf{S}}(i) + \vec{\mathbf{S}}(i) \cdot \frac{\partial \mathbf{A}(ii)}{\partial Q_{\alpha\mathbf{q}}} \cdot \vec{\mathbf{I}}(i) + \\ & + \sum_j^{N_s} \vec{\mathbf{S}}(i) \cdot \frac{\partial \mathbf{D}^{\text{dip}}(ij)}{\partial Q_{\alpha\mathbf{q}}} \cdot \vec{\mathbf{S}}(j). \end{aligned} \quad (9)$$

A $3 \times 3 \times 3$ super-cell containing 1620 atoms is optimised at the density functional theory (DFT) level and it is used to compute the lattice vibrational properties. The molecular optimised structure has been further employed for the calculation of all the spin-phonon coupling coefficients appearing in Eq. (9). The details about the protocol used for the phonons and spin-phonon calculations can be found in the Method Section. All these

interactions break the single-spin time-reversal symmetry and are potentially active in intra-Kramer-doublet spin relaxation, but the physics beyond the three processes is quite different. In order to make these differences more evident we have calculated the spin-phonon coupling squared norms V_{sph}^2 (defined in the Methods section) associated to each phonon modes and their corresponding distributions. The results, reported in panels (b) through (d) of Fig. 1, show striking differences both in qualitative and quantitative terms.

The anisotropy of the spin Hamiltonian is the fingerprint of the dependence of spin degrees of freedom on atomic positions and the same interactions contributing to magnetic anisotropy are also contributing to the derivatives of Eq. 9. The tensors \mathbf{g} and \mathbf{A} have anisotropic components coming from spin-orbit coupling and other interactions localized on the Vanadium centre. Such short-ranged interactions are only influenced by localized intra-molecular vibrations and local rotations affecting the first coordination sphere. In this case, high-energy phonons are still operative. Conversely, dipolar interactions act between different molecules and are both non-local and long-wavelength in nature. These are expected to be prominently modulated by molecular translations. Their interaction thus vanishes at high frequency.

C. VO(acac)₂ Crystal Spin Dynamics

The spin-phonon coupling coefficients discussed in the previous section have been used together with Eq. (6) to simulate the spin dynamics of three different systems: one single electronic spin, one electronic spin interacting with the V nuclear spin and two interacting electronic

spins. Tests including more than two coupled electronic spins are reported in the supplementary information (SI) and show a very small dependence of the relaxation time, τ , on spins farther than the first-neighbour ones. In all simulations, spins are interacting with all the phonons of the periodic crystal, calculated by integrating the Brillouin zone with homogeneous grids up to $64 \times 64 \times 64$ k -points.

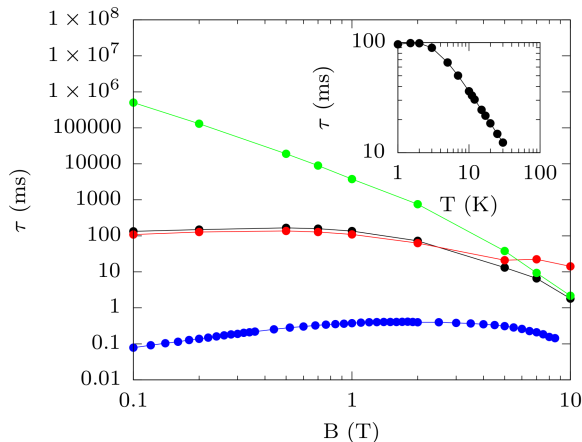


FIG. 2. Spin Relaxation time as function of the B field and the temperature for one electronic spin coupled to one nuclear spin. The relaxation time, τ , in ms as a function of the external field in Tesla is reported for the simulations of one electronic spin coupled to one nuclear spin and relaxing due to the phonons modulation of the Zeeman and hyperfine energies (black line and dots). The contribution coming from the sole hyperfine energy modulation is reported with a red line and dots, while the sole Zeeman contribution is reported by the green line and dots. The experimental relaxation time as extracted from AC magnetometry [19] is also reported (blue dots and line). The inset describes the simulated temperature dependence of spin relaxation at 5 Tesla.

Fig. 2 shows the spin relaxation time as function of the external magnetic field \vec{B} at 20 K for a single electronic spin coupled to the V nuclear spin. The combined effect of the Zeeman and hyperfine modulation, described by the black line and dots, shows a field dependence approaching $|\vec{B}|^4$ in the high field limit ($B > 5$ T), where τ starts to converge to the experimental value [19]. The green curve in Fig. 2, relative to the single electronic spin contribution, shows that in this regime the leading mechanism is the modulation of the Zeeman energy. In the low-field regime the relaxation time as a function of field approaches a plateau where it is about three orders of magnitude longer than the experimental value. The red curve in Fig. 2 shows that the rate-determining mechanism in this regime is the modulation of the hyperfine Hamiltonian.

Numerical tests concerning the effects of the numerical noise in the calculation of the frequencies and the spin-phonon coupling parameters are reported in the SI and prove the robustness of our results. However, it is

important to remark that the energies at play in the low-field regime ($B < 1$ T) are extremely small, if compared with the phonons frequencies and the simulations. Thus, a more sophisticated Brillouin-zone integration scheme might be needed to obtain a more robust estimate of the relaxation times in this field regime. Nonetheless, the calculated relaxation time for low fields is orders of magnitude longer than the experimental one, suggesting the presence of higher-order relaxation mechanisms at play in this regime.

The inset of Fig. 2 displays the temperature dependence of the spin relaxation time in a field of 5 T. In contrast to the experimental results, which show $\tau \propto T^{-n}$ (with $n > 2$) [19], in this field range we simulate a T^{-1} behaviour. Our result is in agreement with what expected from a first-order approximation to spin-phonon coupling and a harmonic lattice dynamics. Deviations from the T^{-1} power law can be considered as fingerprints of higher-order processes taking place. Interestingly, our simulations also show a residual T -independent process in the $T \rightarrow 0$ limit. In this regime, due to the absence of populated phonons states, the only possible relaxation pathway is provided by the T -independent spontaneous phonons emission from a spin excited state. This phenomenon has been recently observed in N-V centres [17].

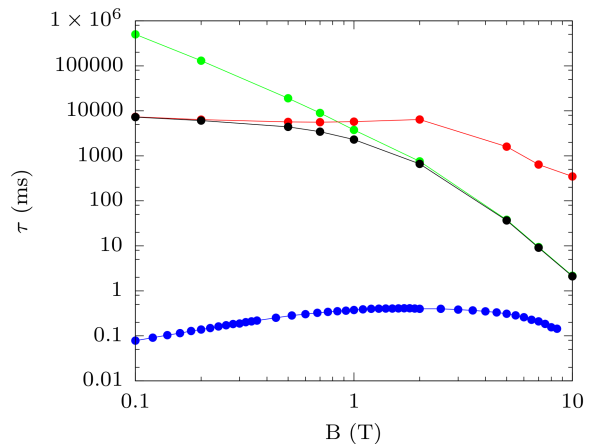


FIG. 3. Spin relaxation time as function of external field for two coupled electronic spins. The relaxation time, τ , in ms as a function of the external field in Tesla is reported for the simulations of two electronic spins relaxing due to the phonons modulation of the Zeeman and dipolar energies (black line and dots). Green line and dots represent the relaxation time of two isolated spins, where only the Zeeman energy is modulated by phonons. The contribution coming from the sole dipolar energy modulation is reported with red line and dots. The experimental relaxation time as extracted from AC magnetometry [19] is also reported (blue dots and line).

Fig. 3 presents the spin-relaxation time as function of the external magnetic field at 20 K for two coupled electronic spins. At high fields ($B < 1$ T) the simulated relaxation dynamics, including both inter- and intra-spin

direct relaxation mechanisms (black curve and dots in Fig. 3), shows no significant difference from that of two isolated spins relaxing through the modulation of the Zeeman interaction (green curve and dots in Fig. 3). The relaxation time due to the sole dipolar contribution (red curve and dots in Fig. 3) becomes predominant only at low fields and it is found to be two orders of magnitude slower than that associated to the hyperfine coupling.

In order to understand the nature of the interaction between $S = 1/2$ spins and the lattice, it is now necessary to look at the nature of the phonons involved in the process. It has been shown that, in the absence of spin-spin interactions, spin relaxation can only occur through the modulation of the spin Hamiltonian by local rotations and intra-molecular distortions [14]. However, for a spin 1/2 in reasonable external fields, the Zeeman spin splitting (up to a few cm^{-1}) is much smaller than the first Γ -point optical mode, here around 50 cm^{-1} . Energy conservation [see Eq. (8)] leaves only acoustic phonons as candidates for the spin-phonon interaction, suggesting that no energy exchange between lattice and spin is possible under these conditions. The solution of this conundrum is provided by the analysis of the phonons nature by means of their decomposition into local molecular translation, local molecular rotations and intra-molecular distortions [14]. The results of this analysis, carried out over the phonons in the entire Brillouin zone, are summarized in Fig. 4, where the total and decomposed phonons density of states are reported.

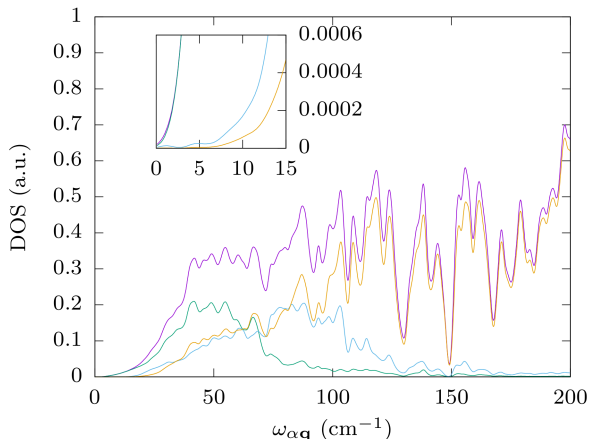


FIG. 4. **Phonons density of states.** In purple it is reported the total phonons density of states as a function of the frequency. The total phonons density of states has been also decomposed in a pure translational contribution (green line), a rotational contribution (blue line) and an intra-molecular contribution (yellow line), all relative to a single molecule inside the unit-cell. The inset shows the details of the density of states in the low energy part of the spectrum. The Brillouin zone has been integrated with a uniform mesh of 64^3 points. The reported density has been smeared with a Gaussian function with breadth 1.0 cm^{-1} .

The total phonons density of states, shows the typ-

ical $\sim\omega^2$ dependence at low frequency, where acoustic phonons dominate the vibrational spectra. However, the decomposition of these modes shows that at low frequency the nature of the acoustic modes is far from being that of a pure molecular translation. A significant rotational and intra-molecular contribution is present at frequencies corresponding to the energy levels' Zeeman splitting considered in this work. These contributions provide an efficient relaxation pathway even for a single spin isolated from other magnetic centres.

II. DISCUSSION

The results of the first-principle calculations presented here are in agreement with Van Vleck's interpretation of the spin relaxation in high fields, where a direct relaxation mechanism due to the Landé tensor modulation is the relevant relaxation pathway. Most importantly we have here demonstrated the mechanism underlying the energy transfer between phonons and spins. The presence of an intra-molecular contribution inside the low-energy acoustic phonons is of fundamental importance in order to open a relaxation channel, that otherwise would be completely inactive due to the translational invariance of the spin-orbit coupling interaction.

The presence of intra-molecular components in acoustic modes can be understood as a mixing between rigid reticular translations and soft molecular modes and it can be used as a rationale to engineer solid-state qubits. More rigid molecular modes are expected to diminish sensibly the contamination of low-energy modes, therefore, extending the spin lifetime. Such a synthetic strategy has been recently attempted [25, 26] on the basis of similar observations for high-spin molecular magnets [14].

To conclude, we have presented a general and fully first-principles method to study spin-lattice dynamics in magnetic materials. We have predicted the correct spin relaxation time and field dependence for a solid-state molecular qubit in high external fields. In particular, we have given, for the first time, a full microscopic rationale of the spin relaxation in solid-state molecular qubits by ranking the three fundamental interactions at play among electronic and nuclear spins at the first order of perturbation theory. Details concerning the spin dynamics at low fields and the nature of the polynomial dependence of the relaxation rate at high- T [19] remain elusive, suggesting the presence of higher-order processes taking place. The method presented here can readily be extended to include higher-order processes such as Raman relaxation mechanism and phonon-phonon interactions. This will be the subject of future work.

III. METHODS

A. Lattice Dynamics

All the structural optimisation and Hessian calculations have been performed with the CP2K software [27] at the level of density functional theory (DFT) with the PBE functional including Grimme's D3 van der Waals corrections [28, 29]. A double-zeta polarised (DZVP) MOLOPT basis set and a 600 Ry of plane-wave cutoff have been used for all the atomic species. The comparison between simulated and experimental lattice parameters is available in ESI. All the translational symmetry independent force constants have been computed by finite difference approach with a 0.01 Å step. Being $\Phi_{ij}(lm)$ the force constant, coupling the i -th atomic degrees of freedom in the lattice cell at the position R_l and the j -th atomic degrees of freedom in the lattice cell of position R_m , the dynamical matrix, $\mathbf{D}(\mathbf{q})$, at the \mathbf{q} -point, is built as

$$D_{ij}(\mathbf{q}) = \sum_l \Phi_{ij}^{l0} e^{i\mathbf{q}\cdot\mathbf{R}_l}. \quad (10)$$

The eigenvalues of $\mathbf{D}(\mathbf{q})$ are $\omega^2(\mathbf{q})$, while the eigenvectors $\mathbf{L}(\mathbf{q})$ defines the normal modes of vibration. The calculated phonons are in good agreement with those previously performed at the sole Γ -point[19].

B. Spin-Phonon Coupling Coefficients

The ORCA software [30] has been employed for the computation of the \mathbf{g} and \mathbf{A} tensors for both equilibrium and distorted geometries. We have used the basis sets def2-TZVP for V and O, def2-SVP for C and H and a def2-TZVP/C auxiliary basis set for all the elements. For the calculation of the \mathbf{A} tensors the entire basis set have been de-contracted. The calculations of the \mathbf{g} tensors have been carried out at the CASSCF+NEVPT2 level of theory, with a (1,5) active space and spin-orbit contributions included through quasi-degenerate perturbation theory. The calculations of the \mathbf{A} tensors have been performed at the DFT level with the PBE functional [28].

The spin phonon coefficients relative to the \mathbf{g} and \mathbf{A} tensors have been calculated as numerical derivatives. Ten Cartesian displacements ranging from ± 0.01 Å, have been used to estimate $\partial\mathbf{g}/\partial X_{is}$ and $\partial\mathbf{A}/\partial X_{is}$, where X_{is} refers to the s Cartesian component of the i -th atom in the DFT optimized unit-cell. The \mathbf{g} vs X_{is} and \mathbf{A} vs X_{is} profiles have been fitted with a fourth order polynomial expression and set to zero if the fitting error on the linear term exceeded 7%. The spin-phonon coupling coefficients relative to the point-dipole-dipole interaction have been obtained by analytical differentiation. The Cartesian derivatives $\partial\hat{H}_s/\partial X_{is}$ have then projected onto the

normal modes by means of the expression

$$\left(\frac{\partial H_s}{\partial Q_{\alpha\mathbf{q}}}\right) = \sum_l^{N_{\text{cells}}} \sum_{is}^{N,3} \sqrt{\frac{\hbar}{N_q \omega_{\alpha\mathbf{q}} m_i}} e^{i\mathbf{q}\cdot\mathbf{R}_l} L_{is}^{\alpha\mathbf{q}} \left(\frac{\partial H_s}{\partial X_{is}^l}\right), \quad (11)$$

where X_{is}^l is the s Cartesian coordinate of the i -th atom of N with mass m_i , inside the unit-cell replica at position \mathbf{R}_l , and N_q is the number of q -points used. All the data regarding spin Hamiltonian parameters and their differentiation are reported in ESI. The spin-phonon coupling distributions have been calculated starting from the spin-phonon coupling coefficients squared norm, defined as

$$V_{\text{sp}}^2(\omega_\alpha) = \frac{1}{N_q} \sum_{\mathbf{q}} \sum_{ij} \left(\frac{\partial g_{ij}}{\partial Q_{\alpha\mathbf{q}}}\right)^2, \quad (12)$$

and analogously for the \mathbf{A} and \mathbf{D}^{Dip} tensors. The Dirac's Delta function appearing in Eq. (8) has been evaluated as a Gaussian function in the limit for infinite q -points and vanishing Gaussian breadth. A grid of 64^3 q -points and a Gaussian breadth of 1 cm^{-1} was estimated to accurately reproduce this limit for all the temperature and field values investigated. Some results about these convergence tests are reported in ESI.

Supplementary Information

Supplementary information is available: the entire form of the non-secular Redfield equations, comparison between experimental and calculated spin Hamiltonian parameters and crystallographic parameters, the spin Hamiltonian parameters for all molecular distortions and relaxation time convergence tests.

Data Availability

All the relevant data discussed in the present paper are available from the authors upon request.

Acknowledgments

This work has been sponsored by Science Foundation Ireland (grant 14/IA/2624). Computational resources were provided by the Trinity Centre for High Performance Computing (TCHPC) and the Irish Centre for High-End Computing (ICHEC). We acknowledge Dr. Lorenzo Tesi and Prof. Roberta Sessoli for providing the original experimental data and the stimulating scientific discussions. We also acknowledge the MOLSPIN COST action CA15128.

Author contributions

All the authors contributed to the discussion of the results and to the manuscript.

Competing financial interests

The authors declare no competing financial interests.

- [1] Peter Caravan, “Strategies for increasing the sensitivity of gadolinium based MRI contrast agents,” *Chem. Soc. Rev.* **35**, 512–523 (2006).
- [2] R. Sessoli, D. Gatteschi, a. Caneschi, and M. a. Novak, “Magnetic bistability in a metal-ion cluster,” *Nature* **365**, 141–143 (1993).
- [3] Gopalakrishnan Balasubramanian, Philipp Neumann, Daniel Twitchen, Matthew Markham, Roman Kolesov, Norikazu Mizuochi, Junichi Isoya, Jocelyn Achard, Johannes Beck, Julia Tissler, Vincent Jacques, Philip R. Hemmer, Fedor Jelezko, and Jörg Wrachtrup, “Ultralong spin coherence time in isotopically engineered diamond,” *Nat. Mater.* **8**, 383–387 (2009).
- [4] Joseph M. Zadrozny, Jens Niklas, Oleg G. Poluektov, and Danna E. Freedman, “Millisecond Coherence Time in a Tunable Molecular Electronic Spin Qubit,” *ACS Cent. Sci.* **1**, 488–492 (2015).
- [5] K. Bader, M. Winkler, and J. van Slageren, “Tuning of molecular qubits: very long coherence and spin–lattice relaxation times,” *Chem. Commun.* **52**, 3623–3626 (2016).
- [6] Samuel J Whiteley, Gary Wolfowicz, Christopher P Anderson, Alexandre Bourassa, He Ma, Meng Ye, Gerwin Koolstra, Kevin J Satzinger, Martin V Holt, F Joseph Heremans, Andrew N Cleland, David I Schuster, Giulia Galli, and David D Awschalom, “Spin–phonon interactions in silicon carbide addressed by Gaussian acoustics,” *Nat. Phys.* (2019), 10.1038/s41567-019-0420-0.
- [7] Ivar Waller, “I. Waller, *Z. Physik* 104, 132 (1936),” *Z. Phys.* **104**, 132 (1936).
- [8] JH Van Vleck, “Paramagnetic relaxation times for titanium and chrome alum,” *Phys. Rev.* (1940).
- [9] R Orbach, “Spin-lattice relaxation in rare-earth salts,” *Proc. R. Soc. A* **264**, 458–484 (1961).
- [10] Silvia Gómez-Coca, Ainhoa Urtizberea, Eduard Cremades, Pablo J Alonso, Agustín Camón, Eliseo Ruiz, and Fernando Luis, “Origin of slow magnetic relaxation in Kramers ions with non-uniaxial anisotropy,” *Nat. Commun.* **5**, 4300 (2014).
- [11] Frank Neese, Mihail Atanasov, Giovanni Bistoni, Dimitrios Manganas, and Shengfa Ye, “Chemistry and Quantum Mechanics in 2019 – Give us Insight and Numbers,” *J. Am. Chem. Soc.* (2019), 10.1021/jacs.8b13313.
- [12] Stefano Curtarolo, Gus L.W. Hart, Marco Buongiorno Nardelli, Natalio Mingo, Stefano Sanvito, and Ohad Levy, “The high-throughput highway to computational materials design,” *Nat. Mater.* **12**, 191–201 (2013).
- [13] Alessandro Lunghi, Federico Totti, Roberta Sessoli, and Stefano Sanvito, “The role of anharmonic phonons in under-barrier spin relaxation of single molecule magnets,” *Nat. Commun.* **8**, 14620 (2017).
- [14] Alessandro Lunghi, Federico Totti, Stefano Sanvito, and Roberta Sessoli, “Intra-molecular origin of the spin-phonon coupling in slow-relaxing molecular magnets,” *Chem. Sci.* **8**, 6051–6059 (2017).
- [15] L. Escalera-Moreno, N. Suaud, A. Gaita-Ariño, and E. Coronado, “Determining Key Local Vibrations in the Relaxation of Molecular Spin Qubits and Single-Molecule Magnets,” *J. Phys. Chem. Lett.* **8**, 1695–1700 (2017).
- [16] Conrad A.P. Goodwin, Fabrizio Ortu, Daniel Reta, Nicholas F. Chilton, and David P. Mills, “Molecular magnetic hysteresis at 60 kelvin in dysprosocenium,” *Nature* **548**, 439–442 (2017).
- [17] T. Astner, J. Gugler, A. Angerer, S. Wald, S. Putz, N. J. Mauser, M. Trupke, H. Sumiya, S. Onoda, J. Isoya, J. Schmiedmayer, P. Mohn, and J. Majer, “Solid-state electron spin lifetime limited by phononic vacuum modes,” *Nat. Mater.* **17**, 313–317 (2018), arXiv:1706.09798.
- [18] Duncan H. Moseley, Shelby E. Stavretis, Komalavalli Thirunavukkuarasu, Mykhaylo Ozerov, Yongqiang Cheng, Luke L. Daemen, Jonathan Ludwig, Zhengguang Lu, Dmitry Smirnov, Craig M. Brown, Anup Pandey, A. J. Ramirez-Cuesta, Adam C. Lamb, Mihail Atanasov, Eckhard Bill, Frank Neese, and Zi Ling Xue, “Spin-phonon couplings in transition metal complexes with slow magnetic relaxation,” *Nat. Commun.* **9**, 1–11 (2018).
- [19] Lorenzo Tesi, Alessandro Lunghi, Matteo Atzori, Eva Luccacini, Lorenzo Sorace, Federico Totti, and Roberta Sessoli, “Giant spin-phonon bottleneck effects in evaporable vanadyl-based molecules with long spin coherence,” *Dalt. Trans.* **45**, 16635–16645 (2016).
- [20] Matteo Atzori, Lorenzo Tesi, Elena Morra, Mario Chiesa, Lorenzo Sorace, and Roberta Sessoli, “Room-Temperature Quantum Coherence and Rabi Oscillations in Vanadyl Phthalocyanine: Toward Multifunctional Molecular Spin Qubits,” *J. Am. Chem. Soc.* **138**, 2154–2157 (2016).
- [21] A. J. Daley, C. Kollath, U. Schollwoeck, and G. Vidal, “Time-dependent density-matrix renormalization-group using adaptive effective Hilbert spaces,” *J. Stat. Mech. Theory Exp.* **P04005**, 1–28 (2004).
- [22] Ilya Kuprov, Nicola Wagner-Rundell, and P. J. Hore, “Polynomially scaling spin dynamics simulation algorithm based on adaptive state-space restriction,” *J. Magn. Reson.* **189**, 241–250 (2007).
- [23] F. Petruccione and H.P. Breuer, *Theory of open quantum system* (2002).
- [24] Matteo Atzori, Lorenzo Tesi, Stefano Benci, Alessandro Lunghi, Roberto Righini, Andrea Taschin, Renato Torre, Lorenzo Sorace, and Roberta Sessoli, “Spin Dynamics and Low Energy Vibrations: Insights from Vanadyl-Based Potential Molecular Qubits,” *J. Am. Chem. Soc.* **139**, 4338–4341 (2017).
- [25] Matteo Atzori, Stefano Benci, Elena Morra, Lorenzo Tesi, Mario Chiesa, Renato Torre, Lorenzo Sorace, and Roberta Sessoli, “Structural Effects on the Spin Dynamics of Potential Molecular Qubits,” *Inorg. Chem.* **57**, 731–740 (2018).
- [26] Tsutomu Yamabayashi, Matteo Atzori, Lorenzo Tesi, Goulven Cosquer, Fabio Santanni, Marie Emmanuelle Boulon, Elena Morra, Stefano Benci, Renato Torre, Mario Chiesa, Lorenzo Sorace, Roberta Sessoli, and Masahiro Yamashita, “Scaling Up Electronic Spin Qubits into a Three-Dimensional Metal-Organic Framework,” *J. Am. Chem. Soc.* **140**, 12090–12101 (2018).
- [27] Joost VandeVondele, Matthias Krack, Fawzi Mohamed, Michele Parrinello, Thomas Chassaing, and Jürg Hutter, “Quickstep: Fast and Accurate Density Functional Calculations Using a Mixed Gaussian and Plane Waves Approach,” *Comput. Phys. Commun.* **167**, 103–128 (2005).
- [28] John P JP Perdew, Kieron Burke, and Yue Wang,

- “Generalized gradient approximation for the exchange-correlation hole of a many-electron system,” *Phys. Rev. B* **54**, 533–539 (1996).
- [29] Stefan Grimme, Jens Antony, Stephan Ehrlich, and Helge Krieg, “A Consistent and Accurate Ab Initio Parametrization of Density Functional Dispersion Correction (DFT-D) for the 94 Elements H-Pu.” *J. Chem. Phys.* **132**, 154104 (2010).
- [30] Frank Neese, “The ORCA program system,” *Wiley Interdiscip. Rev. Comput. Mol. Sci.* **2**, 73–78 (2012).

SUPPLEMENTARY NOTE 1. NON-SECULAR REDFIELD EQUATIONS.

The master matrix for the non-secular Redfield equations is

$$R_{ab,cd}^{\alpha\mathbf{q}} = \frac{\pi}{2\hbar^2} \left[V_{ac}^{\alpha\mathbf{q}} V_{db}^{\alpha\mathbf{q}} \left(G(\omega_{db}, \omega_{\alpha\mathbf{q}}) + G(\omega_{cd}, \omega_{\alpha\mathbf{q}}) \right) - \sum_j \left(V_{aj}^{\alpha\mathbf{q}} V_{jc}^{\alpha\mathbf{q}} \delta_{bd} G(\omega_{jc}, \omega_{\alpha\mathbf{q}}) + V_{dj}^{\alpha\mathbf{q}} V_{jb}^{\alpha\mathbf{q}} \delta_{ca} G(\omega_{jd}, \omega_{\alpha\mathbf{q}}) \right) \right], \quad (1)$$

For a spin Hamiltonian containing N terms, *e.g.* $H_s = \sum_i H_i$, the terms $V_{ac}^{\alpha\mathbf{q}} V_{db}^{\alpha\mathbf{q}}$ appearing in Eq. 1 contains all possible cross-product

$$V_{ac}^{\alpha\mathbf{q}} V_{db}^{\alpha\mathbf{q}} = \sum_{ij} \langle a | \frac{\partial H_i}{\partial Q_{\alpha\mathbf{q}}} | c \rangle \langle d | \frac{\partial H_j}{\partial Q_{\alpha\mathbf{q}}} | b \rangle. \quad (2)$$

In our implementation we only considered the same-index terms. This correspond to assuming that the modulation of each term occurs independently from the others.

SUPPLEMENTARY NOTE 2. LATTICE PARAMETERS AND SPIN HAMILTONIAN.

Supplementary Table 1 reports the calculated and experimental lattice parameters. Taking into account an expected volume reduction due to the absence of temperature expansion in the simulations, the agreement between experimental and calculated ones is excellent.

Model	a (Å)	b (Å)	c (Å)	α (°)	β (°)	γ (°)
Exp ^a	7.346	8.149	11.207	72.86	72.20	66.94
Simulated	7.060	7.935	11.091	74.467	72.622	68.216

^a Taken from Ref. [1].

Supplementary Table 1. **Lattice parameters for the VO(acac)₂ molecular crystal.** The X-ray experimental lattice parameters are compared with those obtained from the periodic DFT optimization of 3x3x3 super-cell.

Supplementary Table 2 reports the comparison between simulated and experimental values of the spin Hamiltonian parameters. Both symmetry and magnitude of the eigenvalues of Landè and Hyperfine tensors are well reproduced. The \mathbf{g} tensor anisotropy is slightly overestimated. On the contrary, the eigenvalues of the \mathbf{A} tensor are slightly underestimated. The order of magnitude of these interactions is however well reproduced and we believe that these differences between calculated and experimental values cannot significantly bias our results.

Model	g_x	g_y	g_z	$ A_x $ (cm ⁻¹)	$ A_y $ (cm ⁻¹)	$ A_z $ (cm ⁻¹)
Exp ^a	1.9845	1.981	1.9477	0.00580	0.00627	0.01712
Simulated	1.9830	1.9814	1.9274	0.00354	0.00396	0.01396

^a Taken from Ref. [1].

Supplementary Table 2. **Spin Hamiltonian parameters for VO(acac)₂.** The spin Hamiltonian experimental parameters are compared with first-principles ones.

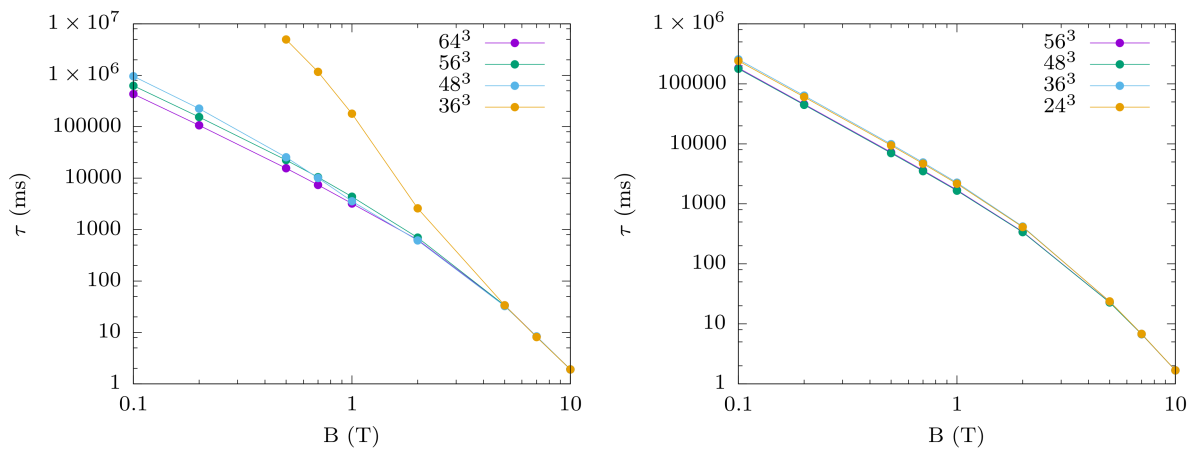
SUPPLEMENTARY NOTE 4. K-POINTS AND PHONON'S LINE-WIDTH CONVERGENCE.

In this work we investigated the harmonic phonons limit of the spin dynamics. In this limit, the phonons's green function contains a Dirac's delta distribution $\delta(\omega - \omega_{\alpha\mathbf{q}})$ that enforces energy conservation. The evaluation of the phonons' Green function requires two numerical approximations. One concerns the use of a discrete number of k-points, in principles infinite due to the infinite extension of a crystalline solid, and the approximation of the Dirac's delta distribution in terms of a regular function.

A Gaussian function converges to a Dirac's delta for a Gaussian breadth approaching 0.

$$\frac{1}{\sigma\sqrt{\pi}}e^{-\frac{(\omega-\omega_{\alpha\mathbf{q}})^2}{\sigma^2}} \xrightarrow{\sigma \rightarrow 0} \delta(\omega - \omega_{\alpha\mathbf{q}}) \quad (3)$$

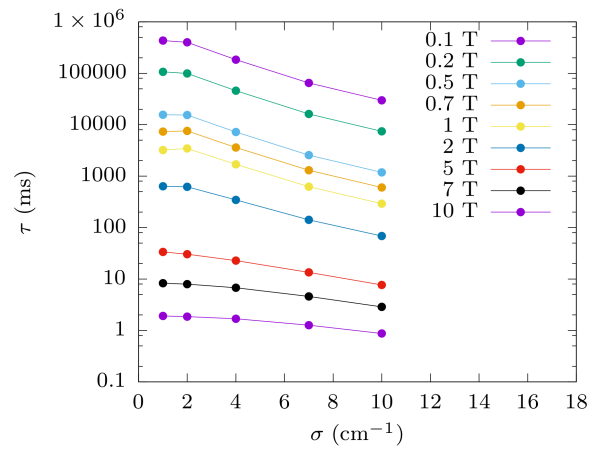
However, this is only true assuming an infinitely dense number of states as function of phonons' frequency. Numerically, this requires the number of k-points to be large enough to guarantee an approximately infinite number of states inside the energy window selected by σ . Therefore, for each value of σ , spin relaxation time must be first converged with respect to the number of k-points. Then, sigma is gradually reduced until relaxation time is converged with respect to this quantity as well.



Supplementary Figure 1. **Spin relaxation time as function of external fields for different values of k-points.** The relaxation time, τ , in ms as function of the Gaussian smearing σ for different values of external field magnitude is reported. The simulation corresponds to the dynamics of one electronic spin relaxing due to the phonons modulation of the Zeeman term of the spin Hamiltonian. The left panel correspond to simulations with $\sigma = 1 \text{ cm}^{-1}$ and the right Panel to simulations with $\sigma = 4 \text{ cm}^{-1}$.

The left panel of Supplementary Figure 1 shows the convergence of τ with respect to the number of k-points when σ is fixed to 1 cm^{-1} . For small Brillouin zone integration grids the spin life-time is largely overestimated. This is because no phonons are available in the near- Γ part of the spectra. Increasing the finess of the integration grid the value converges. For larger values of σ , as reported in the right Panel of Supplementary Figure 1, the convergence is reached for smaller integration grids.

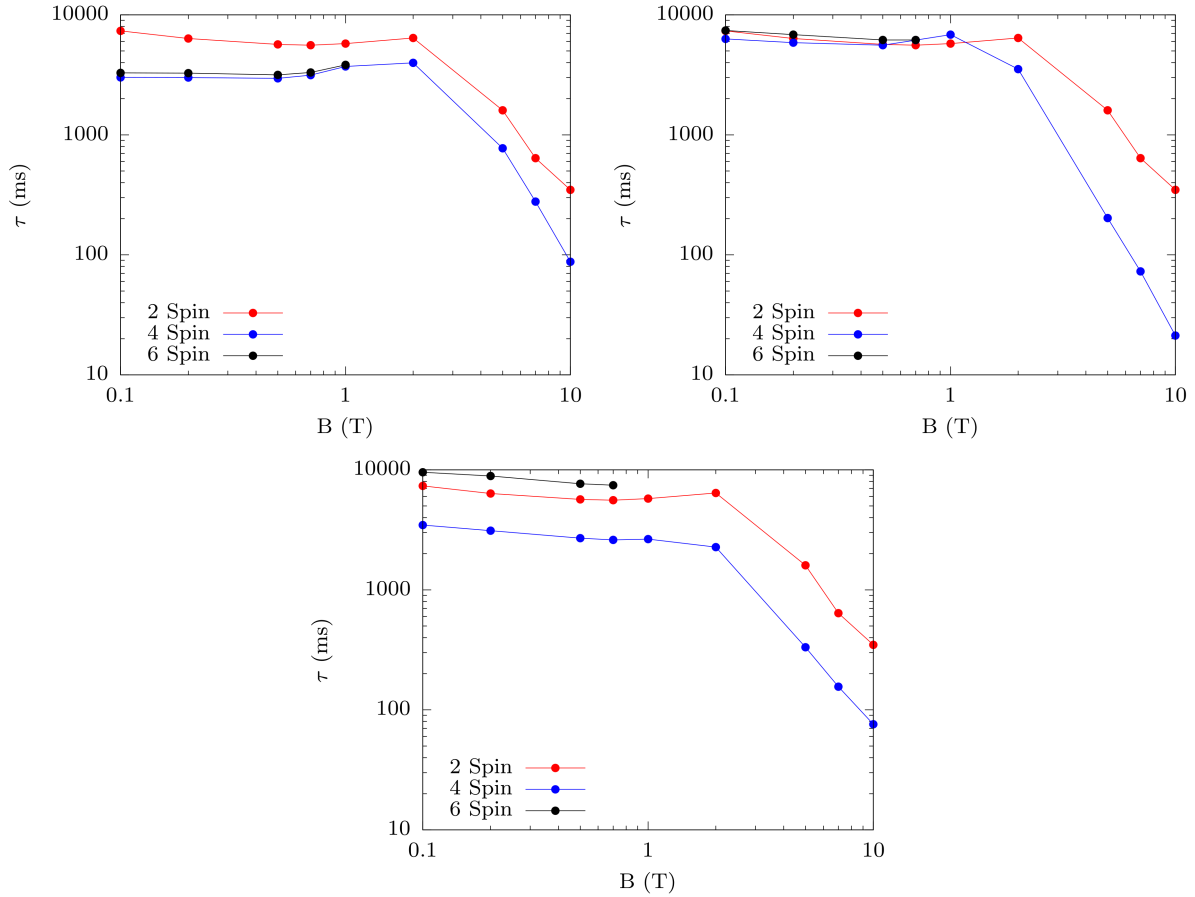
Supplementary Figure 2 reports the dependence of the relaxation time τ with respect to the value σ . For each value of σ the convergence with respect to the number of k-points has been achieved as described above. Relaxation time is nicely converged for $\sigma = 1 \text{ cm}^{-1}$. For smaller values of σ it was not possible to reach convergence on k-points with a reasonable finess of the Brillouin zone integration grid. This is probably due to the fact that an energy window of less than 1 cm^{-1} is small compared to the numerical noise affecting the phonons calculations.



Supplementary Figure 2. **Spin relaxation time as function of the Gaussian breadth for different external fields.** The relaxation time, τ , in ms as function of the Gaussian smearing σ for different values of external field magnitude is reported. The simulation correspond to the dynamics of one electronic spin relaxing due to the phonons modulation of the Zeeman term of the spin Hamiltonian.

SUPPLEMENTARY NOTE 5. NUMBER OF SPINS CONVERGENCE.

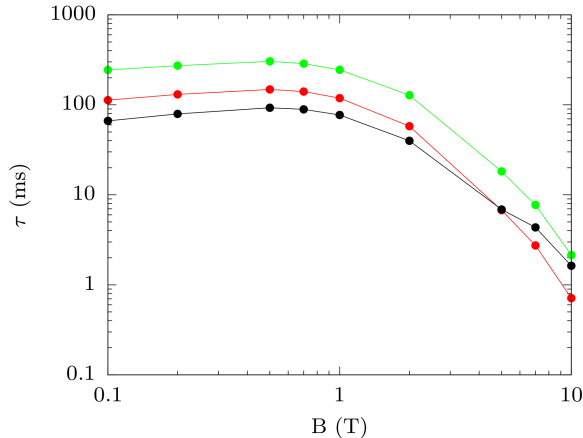
Due to the exponential increase of the dimension of the master matrix in Eq. 1, the study of relaxation time as function of the number of interacting electronic spins has to be restricted to a maximum of six spins. Within this constraint, six different systems can be studied: two and three unit-cells replicated along x,y and z, respectively. The results are summarized in Supplementary Figure 3. The inclusion of multiple electronic spins beyond the first-neighbour one does not dramatically affect the spin dynamics and the estimations of relaxation time made with just two spins correctly capture the essential physics.



Supplementary Figure 3. **Spin relaxation time as function of the number of coupled spins.** The relaxation time, τ , in ms as function of the external field magnitude for different sets of spins is reported: the two spins as in the crystal unit-cell, four spins as obtained by aligning two unit-cells and six spins as obtained by aligning three unit-cells. The top-left Panel shows the results for the reticular direction **a**, top-right Panel shows the results for the reticular direction **b** and the bottom Panel shows the results for the reticular direction **c**.

SUPPLEMENTARY NOTE 6. EFFECT OF NUMERICAL NOISE.

We investigated the effect of numerical noise on the two most important computed quantities: spin-phonon coupling parameters and phonons' frequencies. For the former we studied the effect of multiplying by a factor two all the spin-phonon coupling coefficients relatives to the modulation of the hyperfine Hamiltonian, while for the latter we applied a 20% reduction of all the frequencies. The magnitude of these perturbations has been chosen accordingly to the error these quantities are affected by. In Supplementary Note 2 we have shown that hyperfine parameters are underestimated by a factor of almost two. Comparing our phonons simulations with THz spectroscopy[2] we observe an error on the first frequency at the Γ -point, here calculated at $\sim 50 \text{ cm}^{-1}$, of no more than 20%.



Supplementary Figure 4. **Effect of numerical noise on spin relaxation time.** The relaxation time, τ , in ms as function of the external field magnitude in Tesla for the unbiased case (Green line and dots), for a double hyperfine spin-phonon coupling (Black line and dots) and for a 20% rescaled frequencies (Red line and dots).

Supplementary Figure 4 reports the comparison between the unbiased dynamics (Green line and dots) and the dynamics in presence of a doubled hyperfine interaction (Black line and dots) and the dynamics obtained after frequencies rescaling (Red line and dots). The effect of both the perturbations investigated show that numerical errors in the determination of spin-phonon coupling coefficients and phonons' frequencies do not significantly affect our results and the orders of magnitude of our estimations are well converged.

SUPPLEMENTARY REFERENCES

- [1] Lorenzo Tesi, Alessandro Lunghi, Matteo Atzori, Eva Lucaccini, Lorenzo Sorace, Federico Totti, and Roberta Sessoli, “Giant spin-phonon bottleneck effects in evaporable vanadyl-based molecules with long spin coherence,” *Dalt. Trans.* **45**, 16635–16645 (2016).
- [2] Matteo Atzori, Lorenzo Tesi, Stefano Benci, Alessandro Lunghi, Roberto Righini, Andrea Taschin, Renato Torre, Lorenzo Sorace, and Roberta Sessoli, “Spin Dynamics and Low Energy Vibrations: Insights from Vanadyl-Based Potential Molecular Qubits,” *J. Am. Chem. Soc.* **139**, 4338–4341 (2017).